Structure of Be-13 studied in proton knockout from B-14

Structure of ^{13}Be studied in proton knockout from ^{14}B

G. Ribeiro,[1] E. Nácher,[1,*] O. Tengblad,[1] P. Díaz Fernández,[2,3,4] Y. Aksyutina,[5,6] H. Alvarez-Pol,[3,4] L. Atar,[7,5] T. Aumann,[7,5] V. Avdeichikov,[8] S. Beceiro-Novo,[3,4,9] D. Bemmerer,[10] J. Benlliure,[3,4] C. A. Bertulani,[11] J. M. Boillos,[4] K. Boretzky,[5] M. J. G. Borge,[1] M. Caamano,[3,4] C. Caesar,[7] E. Casarejos,[12] W. Catford,[13] J. Cederkäll,[8] M. Chartier,[14] L. Chulkov,[15,6] D. Cortina-Gil,[3,4] E. Cravo,[16] R. Crespo,[16] U. Datta Pramanik,[17] I. Dillmann,[5] Z. Elekes,[10] J. Enders,[7] O. Ershova,[18] A. Estrade,[5,19] F. Farinon,[5] L. M. Fraile,[20] M. Freer,[21] H. O. U. Fynbo,[22] D. Galaviz,[23] H. Geissel,[5] R. Gernhäuser,[24] P. Golubev,[8] K. Göbel,[25] J. Hagdahl,[2] T. Heftrich,[18] M. Heil,[5] M. Heine,[7] A. Heinz,[2] A. Henriques,[23] M. Holl,[7] A. Hufnagel,[7] A. Ignatov,[7] H. T. Johansson,[2] B. Jonson,[2] N. Kalantar-Nayestanaki,[26] R. Kanungo,[19] A. Kelic-Heil,[5] N. Kurz,[5] T. Kröll,[7] M. Labiche,[27] C. Langer,[18] T. Le Bleis,[24] R. Lemmon,[27] S. Lindberg,[2] J. Machado,[23] J. Marganiec,[6,7,5] A. Movsesyan,[7] T. Nilsson,[2] C. Nociforo,[5] V. Panin,[7,28] S. Paschalis,[7,29] A. Perea,[1] M. Petri,[7,29] S. Pietri,[5] R. Plag,[18] R. Reifarth,[18] C. Rigollet,[26] K. Riisager,[22] D. Rossi,[7,5] M. Röder,[30,31] D. Savran,[6,32] H. Scheit,[7] H. Simon,[5] O. Sorlin,[33] I. Syndikus,[7] J. T. Taylor,[14] R. Thies,[2] P. Velho,[23] A. Wagner,[10] F. Wamers,[5,7] M. Vandebrouck,[34] H. Weick,[5] C. Wheldon,[21] G. Wilson,[35] C. Wimmer,[18] J. S. Winfield,[5] P. Woods,[36] M. V. Zhukov,[2] A. Zilges,[37] and K. Zuber[38]

(R^{3}B Collaboration)

[1]*Instituto de Estructura de la Materia, CSIC, Serrano 113 bis, E-28006 Madrid, Spain*

[2]*Institutionen för Fysik, Chalmers Tekniska Högskola, S-412 96 Göteborg, Sweden*

[3]*Departamento de Física de Partículas, Universidade de Santiago de Compostela, 15706 Santiago de Compostela, Spain*

[4]*IGFAE, Instituto Galego de Física de Altas Enerxías, Universidade de Santiago de Compostela, 15706 Santiago de Compostela, Spain*

[5]*GSI Helmholtzzentrum für Schwerionenforschung, D-64291 Darmstadt, Germany*

[6]*ExtreMe Matter Institute (EMMI), GSI Helmholtzzentrum für Schwerionenforschung GmbH, D-64291 Darmstadt, Germany*

[7]*Institut für Kernphysik, Technische Universität Darmstadt, D-64289 Darmstadt, Germany*

[8]*Department of Physics, Lund University, S-22100 Lund, Sweden*

[9]*National Superconducting Cyclotron Laboratory, Michigan State University, East Lansing, Michigan 48824, USA*

[10]*Helmholtz-Zentrum Dresden-Rossendorf, D-01328 Dresden, Germany*

[11]*Department of Physics and Astronomy, Texas A&M University-Commerce, Commerce, Texas 75429, USA*

[12]*University of Vigo, E-36310 Vigo, Spain*

[13]*Department of Physics, University of Surrey, Guildford GU2 5FH, United Kingdom*

[14]*Oliver Lodge Laboratory, University of Liverpool, Liverpool L69 7ZE, United Kingdom*

[15]*NRC Kurchatov Institute, Ru-123182 Moscow, Russia*

[16]*Departamento de Física, Instituto Superior Técnico, Av Rovisco Pais 1, 1049-001 Lisboa, Portugal*

[17]*Saha Institute of Nuclear Physics, 1/AF Bidhan Nagar, Kolkata-700064, India*

[18]*Goethe-Universität Frankfurt am Main, D-60438 Frankfurt am Main, Germany*

[19]*Astronomy and Physics Department, Saint Mary's University, Halifax, Nova Scotia, Canada, B3H 3C3*

[20]*Facultad de Ciencias Físicas, Universidad Complutense de Madrid, Avda. Complutense, E-28040 Madrid, Spain*

[21]*School of Physics and Astronomy, University of Birmingham, Birmingham B15 2TT, United Kingdom*

[22]*Department of Physics and Astronomy, Aarhus University, DK-8000 Århus C, Denmark*

[23]*Centro de Fisica Nuclear, University of Lisbon, P-1649-003 Lisbon, Portugal*

[24]*Physik Department E12, Technische Universität München, 85748 Garching, Germany*

[25]*Johann Wolfgang Goethe-Universität Frankfurt, Max-von-Laue Strasse 1, 60438 Frankfurt am Main, Germany*

[26]*KVI-CART, University of Groningen, Zernikelaan 25, NL-9747 AA Groningen, Netherlands*

[27]*STFC Daresbury Laboratory, Daresbury, Warrington WA4 4AD, United Kingdom*

[28]*RIKEN, Nishina Center for Accelerator-Based Science, 2-1 Hirosawa, 351-0198 Wako, Saitama, Japan*

[29]*Department of Physics, University of York, York YO10 5DD, United Kingdom*

[30]*Helmholtz-Zentrum Dresden-Rossendorf, Institute of Radiation Physics, P.O.B. 510119, 01314 Dresden, Germany*

[31]*Technische Universität Dresden, Institut für Kern- und Teilchenphysik, Zellescher Weg 19, 01069 Dresden, Germany*

[32]*Frankfurt Institut for Advanced Studies FIAS, Frankfurt, Germany*

[33]*Grand Accélérateur National d'Ions Lourds (GANIL), CEA/DSM-CNRS/IN2P3, B.P. 55027, F-14076 Caen Cedex 5, France*

[34]*GANIL, Bd Henri Becquerel, 14076 Caen, France*

[35]*Department of Physics, University of Surrey, Guildford GU2 5XH, United Kingdom*

[36]*School of Physics and Astronomy, University of Edinburgh, Edinburgh EH9 3JZ, United Kingdom*

[37]*Institut für Kernphysik, Universität zu Köln, D-50937 Köln, Germany*

[38]*Institut für Kern- und Teilchenphysik, Technische Universität, 01069 Dresden, Germany*

(Received 17 May 2018; published 3 August 2018)

The neutron-unbound isotope ^{13}Be has been studied in several experiments using different reactions, different projectile energies, and different experimental setups. There is, however, no real consensus in the interpretation of the data, in particular concerning the structure of the low-lying excited states. Gathering new experimental information, which may reveal the ^{13}Be structure, is a challenge, particularly in light of its bridging role between ^{12}Be, where the $N = 8$ neutron shell breaks down, and the Borromean halo nucleus ^{14}Be. The purpose of the present study is to investigate the role of bound excited states in the reaction product ^{12}Be after proton knockout from ^{14}B, by measuring coincidences between ^{12}Be, neutrons, and γ rays originating from de-excitation of states fed by neutron decay of ^{13}Be. The ^{13}Be isotopes were produced in proton knockout from a 400 MeV/nucleon ^{14}B beam impinging on a CH_2 target. The ^{12}Be-n relative-energy spectrum $d\sigma/dE_{fn}$ was obtained from coincidences between ^{12}Be(g.s.) and a neutron, and also as threefold coincidences by adding γ rays, from the de-excitation of excited states in ^{12}Be. Neutron decay from the first $5/2^+$ state in ^{13}Be to the 2^+ state in ^{12}Be at 2.11 MeV is confirmed. An energy independence of the proton-knockout mechanism is found from a comparison with data taken with a 35 MeV/nucleon ^{14}B beam. A low-lying p-wave resonance in ^{13}Be$(1/2^-)$ is confirmed by comparing proton- and neutron-knockout data from ^{14}B and ^{14}Be.

DOI: 10.1103/PhysRevC.98.024603

I. INTRODUCTION

The chain of known isotopes of the chemical element beryllium, limited by the two unbound $A = 6$ and $A = 16$ nuclei, exhibits some of the most intriguing phenomena among light drip-line nuclei. The interplay between shell-model and cluster structures attracts considerable interest, both experimentally and theoretically.

The $\alpha + \alpha$ cluster structure of ^{8}Be is well established, and there is convincing evidence that clustering persists also in the heavier beryllium isotopes.

The structure of ^{9}Be(g.s.) is expected to be two α particles in a dumbbell configuration coupled to a neutron [1]. There is, however, no complete understanding of the nature of its first excited state, ^{9}Be$(1/2^+)$. It has been described as a resonance [2], a virtual state in ^{8}Be $+ n$ [3,4], or a genuine three-body $\alpha + \alpha + n$ resonance, where the ^{5}He $+ \alpha$ configuration dominates at small distances and ^{8}Be $+ n$ at large distances [5,6]. Another interesting feature of ^{9}Be is a parity inversion, where its $I^\pi = 1/2^+$ state is found at an energy ≈ 1 MeV lower than the $I^\pi = 1/2^-$ state.

Within the framework of the shell model, the ground state of ^{10}Be is dominated by a p-shell configuration, where the (sd) mixing is small [7]. The ^{10}Be(g.s.) structure can also be described using cluster models [8,9]. The motion of the two neutrons around the strongly deformed ^{8}Be core was investigated with a mixing of a minor $(sd)^2$ component into the major p^2 component [9].

The ground state of ^{11}Be was early found [10,11] to have spin parity $I^\pi = 1/2^+$ instead of $I^\pi = 1/2^-$ as predicted by the shell model. An experimental study demonstrated the dominant ^{10}Be $\otimes (1s_{1/2})$ single-particle character of the ^{11}Be ground state [12], but revealed also a contribution from a ^{10}Be$(2^+) \otimes (0d_{5/2})$ admixture [13–15]. The parity inversion anomaly was first discussed in Ref. [16], where it was pointed out that the core excitation to the first 2^+ state and the pairing blocking effect are both important to produce the parity inversion. A recent theoretical study using *ab initio* approaches to nuclear structure shows that only certain chiral interactions are capable of reproducing the parity inversion [17].

Already in 1976 strong configuration mixing in ^{12}Be was predicted by Barker [18]. This enormous breaking of the closed-shell neutron structure in ^{12}Be was confirmed experimentally, when an admixture of about 32% closed p-shell and 68% $(sd)^2$ configurations were determined [19].

In ^{13}Be, which is the subject of our study, a large weight of a ^{10}Be $\otimes (sd)^3$ configuration is expected in the ground-state wave function. ^{12}Be cannot reasonably be considered a closed-shell nucleus, as discussed in many papers about ^{13}Be and ^{14}Be [20–26].

A recent theoretical study shows that the lowest $(sd)^4$ state in ^{14}Be may be quite close to the lowest $(sd)^2$ state [27]. Thus a substantial admixture of a ^{10}Be $\otimes (sd)^4$ component can be expected in the ^{14}Be ground state.

Investigations of the structure of ^{13}Be can provide a bridge to the understanding of ^{14}Be. A review of rather controversial results of experimental and theoretical studies of ^{13}Be was given in Ref. [28] and recently updated in a broader review paper on light nuclei [29].

The experimental information about the structure of ^{13}Be was obtained from studies using two conceptually different experimental approaches:

(1) The *missing-mass method* is used for reconstruction of resonances in the system of particles that were not detected. The method is based on kinematic relations and measured momentum vectors of the incoming beam and the detected particle.
(2) In the *invariant-mass method*, the four-momenta of incoming and detected particles are used to determine the resonance in the system of detected particles. However,

*enrique.nacher@csic.es

when excited, γ-decaying states are populated, and the resonance position is shifted down by the energy of the escaping γ ray.

The missing-mass data for ^{13}Be in Refs. [30–34] are in good agreement. The weighted mean values for the observed resonance energies are at 0.73(7) MeV [33,34], the next at 1.99(4) [30–34] corresponding to the first $5/2^+$ state, and higher excited resonances at 2.92(7) MeV [33,34] and at 5.05(5) MeV [30–34].

There exists, however, quite a strong contradiction between the interpretations of the data obtained in experiments using the invariant-mass method [28]. Based on such measurements the position of the first excited state was suggested to have a resonance energy of 2.39(5) MeV, $0.85^{+0.15}_{-0.11}$ MeV, and 1.05(10) MeV in Refs. [35–37], respectively. Furthermore, the determined widths were 2.4(2) MeV, $0.30^{+0.34}_{-0.15}$ MeV, and 0.50(20) MeV, respectively.

The second $5/2^+_2$ state was suggested at $E_r = 2.35(14)$ MeV ($\Gamma = 1.5(40)$ MeV) [36] and at $E_r = 2.56(13)$ MeV ($\Gamma = 2.29(73)$ MeV) [37]. The determined widths are in both cases more than a factor of 10 larger than the theoretical values given in Ref. [38].

The reason for different interpretations is most likely connected to the need for taking the feeding of excited states in ^{12}Be into account in the analysis. The three lowest excited states are found at 2.11 MeV ($I^\pi = 2^+$), 2.24 MeV ($I^\pi = 0^+_2$, an isomeric state with a lifetime of $\tau = 331(12)$ ns), and 2.71 MeV ($I^\pi = 1^-$) [39–41].

In recent experiments on ^{13}Be, this nucleus was studied with proton knockout from ^{14}B [36] and via nucleon exchange in ^{13}B [37]. It is unlikely that a 1^- state in ^{12}Be would be populated in either of these reactions, while the probabilities of ^{12}Be(2^+) and ^{12}Be(0^+_2) excitations are expected to be comparable [42]. None of these experiments included the detection of possible γ rays from ^{12}Be.

One-neutron knockout from a 69 MeV/nucleon ^{14}Be beam was studied at RIKEN [35]. There, the detection of triple coincidences between fragments, neutrons, and γ rays demonstrated a measurable probability for the population of excited states in ^{12}Be at 2.11 MeV (2^+) and 2.71 MeV (1^-).

In this paper new data are presented, from an experiment studying proton knockout from ^{14}B at 400 MeV/nucleon impinging on a CH_2 target where neutrons, fragments, and γ rays from the ^{13}Be breakup were recorded. The data were taken during the S393 campaign at the GSI Helmholtzzentrum für Schwerionenforschung GmbH by the R^{3}B Collaboration.

II. EXPERIMENTAL SETUP AND DATA ANALYSIS

The radioactive ^{14}B beam was produced in fragmentation reactions of a primary ^{40}Ar beam, with an energy of 490 MeV/nucleon, directed from the heavy-ion synchrotron (SIS18) towards a production target consisting of natural Be (4.011 g/cm^2). The fragments were separated according to their magnetic rigidities in the fragment separator (FRS). The secondary ^{14}B beam, with an energy of 400 MeV/nucleon, impinged on a polyethylene (922 mg/cm^2) reaction target. A schematic view of the experimental setup is shown in Fig. 1. The main feature of this setup is its capability to record four-momentum, mass, and charge of the incoming ions and the outgoing reaction products. To accomplish this task, it is equipped with a large variety of detectors and the dipole-magnet spectrometer ALADIN. Since our results rely on the good performance of the Crystal Ball detector and the Large Area Neutron Detector (LAND), we give a short description of these two key parts of the experimental setup in the following.

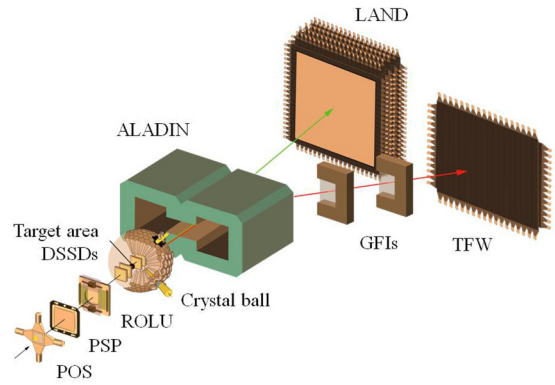

FIG. 1. Schematic view of the experimental setup. The square-shaped plastic scintillator (POS) is used as the start signal of the time-of-flight measurements and gives also information about the energy loss of the beam particles. The position sensitive silicon pin diode (PSP) detectors are used for tracking of the beam position and for determining the charge of the isotopes from their energy loss. The ROLU is a set of scintillators, which allows one to restrict the active beam size. Any particle that does not pass through the hole defined by the position of the four scintillators gives a signal, which is used as a veto trigger for the data acquisition system. Double-sided silicon strip detectors (DSSDs) in front of and behind the reaction target are used for separating the charge and tracking of the emerging fragments. The two fiber detectors (GFIs) are used for tracking the fragment trajectories. A set of scintillators, the time-of-flight wall (TFW), is used to provide a stop signal for the time-of-flight measurement and as an energy loss detector. The LAND neutron detector and the Crystal Ball, surrounding the target, are discussed in the text. Figure from Ref. [43].

Crystal Ball. The Crystal Ball sphere [44], surrounding the target, is a NaI(Tl)-scintillator-crystal assembly with 159 detectors, with an inner radius of 25 cm, and a crystal length of 20 cm. Its geometry follows the requirement of each crystal covering the same solid angle of 77 msr with four different crystal shapes. This detector measures both the γ rays emitted from the nuclear reaction produced in the target, and the protons from the proton-knockout reaction. The sum peak method, using ^{60}Co as a calibration γ source, with energies 1173 and 1332 keV, was applied to determine the efficiency for detection of γ rays by the Crystal Ball [45]. The relatively high segmentation of the Crystal Ball enables Doppler correction of the γ rays emitted by the fragments moving at relativistic energies.

LAND. The Large Area Neutron Detector [46] is located 13 m downstream from the reaction target, straight ahead in the direction of the incoming beam. The size of the detector is 2×2 m^2 with a depth of 1 m, designed to measure both

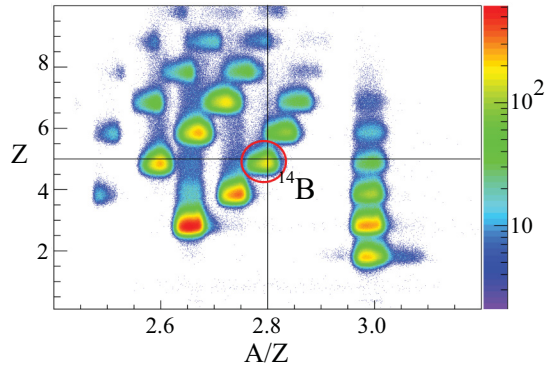

FIG. 2. Fragment identification data of the incoming beam. The ordinate corresponds to the charge (Z) of the incoming isotopes whereas the abscissa is the ratio between mass and charge (A/Z).

time of flight and position of fast neutrons with energies above 150 MeV, providing good momentum resolution. The intrinsic time resolution is 370 ps and the position resolution is 5 cm.

A. Incoming isotope identification

From the fragmentation of the primary ^{40}Ar beam in the Be production target a broad variety of nuclides is produced. The purpose of the FRS is to separate and select the isotopes of interest from the different nuclides produced in the reaction. A cocktail of different nuclei reaches the reaction target. Some of the detectors (e.g., the ones labeled PSP and POS in Fig. 1) are used to select the incoming nucleus of interest during the analysis, ^{14}B in our case, as shown in the fragment identification plot in Fig. 2.

B. Fragment and neutron selection

In order to identify all the emerging fragments according to their charge Z and mass A, we have used the measured energy loss in the two double-sided silicon strip detectors (DSSDs) right after the reaction target and the time-of-flight wall (TFW) after the ALADIN magnet.

C. ^{12}Be-n relative energy spectra and γ rays

The relative energy between ^{12}Be and a neutron (E_{fn}) was determined by the invariant-mass method using the relativistic expression

$$E_{fn} = \|(\mathbf{P}_f + \mathbf{P}_n)\| - M_f - m_n, \quad (1)$$

where $\mathbf{P}_f$ ($\mathbf{P}_n$) and M_f (m_n) are the four-momenta and the masses of the fragment (neutron), respectively.

The experimental resolution of the relative energy spectrum ($d\sigma/dE_{fn}$) was obtained from Monte Carlo simulations using the measured detector responses. The resolution (FWHM) is about 250 keV at 500 keV and increases to about 700 keV at 2 MeV. The Monte Carlo simulations also give the overall detection efficiency. The detection efficiency remains nearly constant, 85%, up to $E_{fn} = 2$ MeV and decreases at higher energies due to the finite solid angle of LAND and the acceptance of the ALADIN magnet. All measured distributions were corrected for the overall detection efficiency.

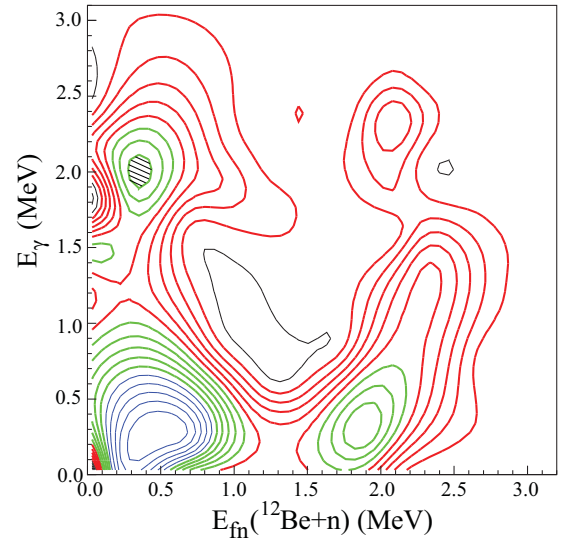

FIG. 3. Contour plot of E_γ as function of E_{fn} after multi-quadratic smoothing of the triple-coincidence data. The maximal intensity is found in the energy region $E_\gamma \sim 2$ MeV and E_{fn} less than 0.5 MeV (hatched area). Note also the events at $E_\gamma \sim 2$ MeV and $E_{fn} \sim 2$ MeV.

An important experimental improvement in the present experiment is that γ rays from excited states in the residual nucleus ^{12}Be, populated in the neutron decay of ^{13}Be, are detected in the Crystal Ball with high efficiency. A two-dimensional spectrum of E_γ as a function of E_{fn} was constructed from the about 2500 recorded events of triple coincidences between γ rays, corrected for their Doppler shift, ^{12}Be, and neutrons. The $E_\gamma(E_{fn})$ distribution after multi-quadric smoothing is shown in Fig. 3. A peak in the γ spectrum (hatched area) is clearly present in this plot at about 2 MeV and E_{fn} less than 0.5 MeV. There are also some events located at $E_\gamma \sim 2$ MeV and $E_{fn} \sim 2$ MeV, indicating an excited state in ^{13}Be at $E_r \sim 4$ MeV decaying into the ^{12}Be(2^+) state.

D. Data analysis and results

The Doppler-corrected γ spectrum measured with the Crystal Ball detector, in coincidence with a ^{12}Be fragment and a neutron, is shown in Fig. 4(a). The spectrum shows a Gaussian-shaped structure in the energy range 2.0–2.3 MeV superimposed on a smooth background. The source of the background is mainly due to secondary particles: protons, neutrons, and δ electrons. The shape of the background agrees rather well with R3BRoot simulations [47]. The solid line displays a fit of the spectrum with $\chi^2/N = 1.11$. Figure 4(b) shows a Gaussian fit to the spectrum after subtraction of the smooth background, giving a centroid of $E_\gamma = 2.16(4)$ MeV, in good agreement with the expected 2.11 MeV γ rays from de-excitation of the first excited 2^+ state in ^{12}Be, $\chi^2/N = 0.83$.

The experimental $d\sigma/dE_{fn}$ spectrum, obtained from coincidences between ^{12}Be fragments and neutrons from this experiment, is shown in Fig. 5(a). There is one data point in

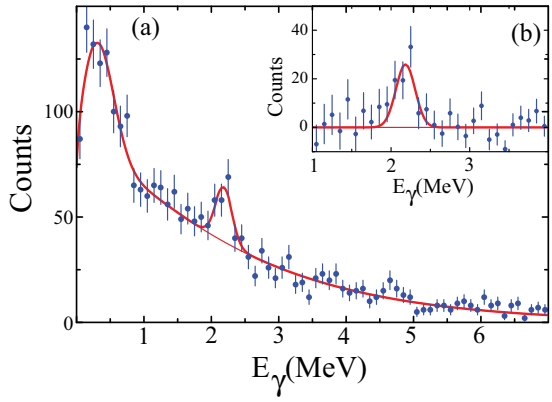

FIG. 4. (a) Doppler-corrected γ spectrum measured with the Crystal Ball detector in coincidence with ^{12}Be and a neutron obtained from a projection of the two-dimensional distribution $E_\gamma(E_{fn})$ in Fig. 3. The centroid of the Gaussian-shaped peak was found to be 2.16(4) MeV with width $\sigma = 168(50)$ keV on the top of a smooth background. This confirms the presence of neutron decay from ^{13}Be to the 2^+ state in ^{12}Be. (b) γ spectrum after background subtraction.

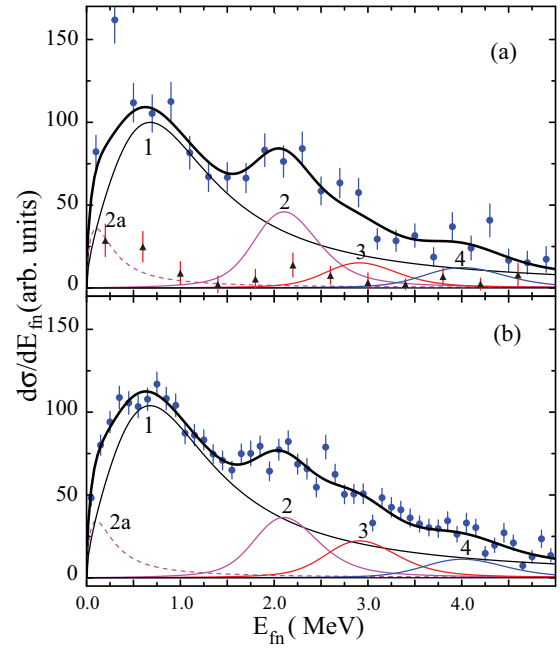

FIG. 5. Experimental spectrum of the relative ^{12}Be-n energy, $d\sigma/dE_{fn}$, obtained in proton knockout from ^{14}B at (a) 400 MeV/nucleon (present data) and (b) 35 MeV/nucleon energies (Ref. [36]). The data are corrected for overall efficiency and normalized to the same integral value. The contributions from the threefold $^{12}\text{Be} + n + \gamma$ coincidences are shown by ▲. The data are corrected for the efficiency of γ detection, 40%. Overlaid on the experimental points, the fit to three Breit-Wigner resonances (thin solid lines: black, pink, red, and blue) and their decay branches to the γ-decaying ^{12}Be(2^+) state (dashed lines). The thick solid black lines show a global fit to the data: (a) $\chi^2/N = 1.0$ and (b) $\chi^2/N = 1.8$. See text for details.

the $d\sigma/dE_{fn}$ spectrum around 0.3 MeV, deviating from the main trend of the neighboring points in the spectrum by about 5σ. With the present experimental resolution we cannot give any physics arguments for this deviation and have therefore neglected the point in the analysis. The spectrum was analyzed using Breit-Wigner-shaped resonances for the different partial waves. The energy dependence of the resonance widths, $\Gamma(E_{fn})$, was taken into account in the analysis according to the R-matrix prescription [48]. The rather smooth and broad shape of the spectrum indicates contributions from several individual, but overlapping, resonances. There would thus be a lack of uniqueness of the analysis if all resonance parameters were taken as free. For this reason, only the position and width of the dominating structures, the $1/2^+$ state and the $5/2^+_1$ state, were left free while other resonance parameters were taken from the missing-mass experiments. The inclusion of one more state at a resonance energy of 4.0 MeV was found to give a considerable reduction of the χ^2/N of the fit, consistent with the evidence shown in Fig. 3. The fit was made using the functional minimization and error analysis code MINUIT [49]. We also used data from an experiment performed at GANIL [36], where the same reaction was studied, but with a 35 MeV/nucleon ^{14}B beam. In experiments using the missing-mass method [31,33,34], the resonances above $E_{fn} = 1$ MeV were found to be narrow, about 0.4 MeV. The energy resolution in the present experiment is given as $\sigma = 0.18E_{fn}^{0.75}$ MeV [50], which corresponds, for example, to FWHM = 0.7 MeV at 2 MeV. Thus, the resonance shapes in the experimental spectra are mainly determined by the experimental resolution, and the intrinsic widths of the resonances were therefore kept fixed during the fit. The results from a simultaneous fit to the two data sets are shown in Figs. 5(a) and 5(b) and in Table I. The parameters for the low-lying $1/2^+$ resonance are within statistical uncertainties close to the result given in Ref. [51]. The rule of thumb is that if $\Gamma < 4E_r$, the state is a real resonance, whereas it becomes virtual if $\Gamma \geqslant 4E_r$ [52].

The parameters of the first $5/2^+$ state are in agreement with the results of the missing-mass experiments. The analysis of the data obtained at 35 and 400 MeV/nucleon with the same resonance parameters results in similar relative population of

TABLE I. Resonance energy E_r (MeV), resonance width Γ (MeV) at the resonance energy, and assumed spin and parity I^π, for the states in the fit of the spectra in Figs. 5(a) and 5(b). The last two columns show the population relative to the $1/2^+$ state $Y/Y_{1/2}$, where the integrations were made in the energy region from 0 to 5 MeV. Statistical uncertainties are given in brackets. The resonance decay to the ^{12}Be(2^+) state is marked by ⇓ and the parameters marked by * are taken from Refs. [31,33,34]; see text.

N	E_r	$\Gamma(E_r)$	I^π	$Y/Y_{1/2^+}$	
				This work	Ref. [36]
1	0.86(4)	1.70(15)	$1/2^+$	1.00	1.00
2a	0.1 ⇓		$5/2^+_1$	0.1	0.1
2	2.11(5)	0.4*	$5/2^+_1$	0.24(4)	0.18(2)
3	2.92*	0.4*	$(5/2^+_2)$	0.09(3)	0.12(2)
4	4.0*	0.4*	$(3/2^+)$	0.08(2)	0.07(2)

resonance states ($Y/Y_{1/2^+}$). This supports the assumption that the reaction mechanism, the proton knockout, remains the same at different energies and targets.

The $d\sigma/dE_{fn}$ spectrum obtained from the $^{12}\mathrm{Be}+n+\gamma$ ray (2.11 MeV) triple-coincidence data [Fig. 5(a)] was also included in the analysis. The corresponding $d\sigma/dE_{fn}$ spectrum was constructed by two methods:

(1) The $d\sigma/dE_{fn}$ spectrum was obtained with the condition $2.0 < E_\gamma < 2.4$ MeV. From this spectrum a background was subtracted by events at the left-hand and right-hand sides of the 2.11 MeV peak: $1.7 < E_\gamma < 2.0$ MeV and $2.4 < E_\gamma < 2.7$ MeV.

(2) The γ spectra obtained in coincidence with ^{12}Be and neutron in different 400 keV energy bins of E_{fn} were fitted by a Gaussian superimposed on a background, as shown in Fig. 4. The parameters of the fit were obtained from the fit to the γ spectrum for the whole energy region $0 < E_{fn} < 6$ MeV [see Fig. 4(b)] and all parameters were kept fixed except for the amplitudes of the Gaussian and the background. The number of events inside the Gaussian component was taken as originating from $^{12}\mathrm{Be}+n+\gamma$ (2.11 MeV) three-body coincidences in the corresponding E_{fn} energy region.

Both methods give, within statistical uncertainties, the same result. The contributions from the triple $^{12}\mathrm{Be}+n+\gamma$ coincidences obtained with the second method are shown in Fig. 5(a) as black triangles (▲).

The interpretation of these results can be summarized as follows: The decay of the s-wave state of ^{13}Be to the ^{12}Be(g.s.) (labeled 1 in Fig. 5) together with a contribution from s-wave neutrons from the upper tail of the first $5/2^+$ excited state feeding of the 2.11 MeV (2^+) state in ^{12}Be (2a) are responsible for the low-energy part of the observed $d\sigma/dE_{fn}$ spectrum. The resonances at 2.11, 2.92, and 4.0 MeV decaying to the ^{12}Be ground state are sufficient to explain the rest of the $d\sigma/dE_{fn}$ spectrum up to 5 MeV.

The structure of the first $5/2^+$ state is predominantly of $^{10}\mathrm{Be}\otimes(sd)^3$ character rather than $^{12}\mathrm{Be}\otimes d_{5/2}$ [53]. Its wave function is mostly given by $^{10}\mathrm{Be}\otimes(0d_{5/2}, 1s^2_{1/2})$. Another competing component is $^{12}\mathrm{Be}(2^+)\otimes 1s_{1/2}$, which could be appreciable [54]. This component can only decay to the 2^+ state of ^{12}Be. The obtained result supports the importance of this component in the structure of the $^{13}\mathrm{Be}(5/2^+_1)$ state. Figure 6 gives the level scheme of ^{13}Be with energies for the positive-parity states taken from the present analysis. The very broad s state ($1/2^+$) dominates the excitation spectrum up to the 2 MeV region. We also show a more narrow p state situated on top of this broad state which has been found in the neutron-knockout data from ^{14}Be [35,51].

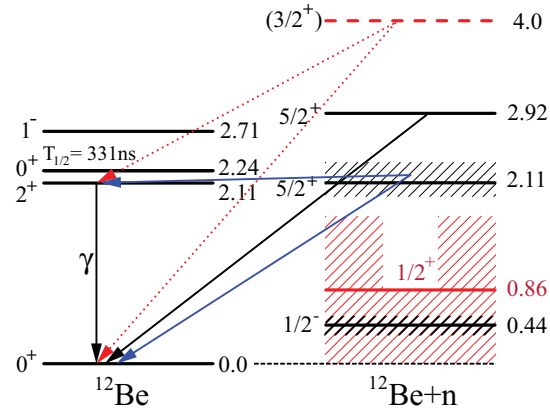

FIG. 6. Proposed level scheme of ^{13}Be together with the neutron decay channels to the ground state and excited states in ^{12}Be. The energies for the positive-parity states are from the present paper, while the low-energy negative-parity state is from neutron-knockout data from ^{14}Be [35,51].

III. DISCUSSION

In experiments adopting the invariant-mass method it is generally assumed that the resonance reveals itself as a final-state interaction between the detected particles. This method has been widely applied in the production and study of ^{13}Be as in fragmentations of ^{18}O [55] and ^{48}Ca [56] and in proton knockout from ^{14}B [36,57], in neutron knockout from ^{14}Be [35,51,58], and in a nucleon exchange reaction with a ^{13}B beam [37]. However, the absence of distinct resonance structures in the present ^{12}Be-n $d\sigma/dE_{fn}$ spectra together with a possible neutron decay to excited states in ^{12}Be leads to uncertainties in interpretations of the experimental data. The use of different reactions allows for significant reduction of ambiguity if all data are taken into account. Such discussions were given in Refs. [35,51,58], but it is clear that there is an absolute need for triple γ-n-^{12}Be data to draw firm conclusions.

The ^{12}Be relative velocities, measured in fragmentation of 40 MeV/nucleon ^{18}O [55] and 60 MeV/nucleon ^{48}Ca [56], give evidence for low-lying s-wave strength in ^{13}Be. However, this observation can also be explained as arising from the decay of the $^{14}\mathrm{Be}(2^+)$ state to ^{12}Be and two neutrons (see Fig. 4 in Ref. [59]).

Figure 7(a), which demonstrates that the shapes of the ^{12}Be-n relative energy spectra obtained in a proton knockout from ^{14}B, at 35 MeV/nucleon [36] and in the present experiment at 400 MeV/nucleon are likewise similar, also indicates an energy independence of the proton-knockout mechanism. The ^{12}Be-n energy spectra measured with the ^{14}Be beam in neutron knockout were also shown to be quite similar at two different energies of the incoming beam, 68 [35] and 360 MeV/nucleon [51], supporting the assumption of an energy-independent neutron-knockout mechanism.

Figure 7(a) also shows a comparison between experimental spectra from proton- and neutron-knockout reactions. The comparison demonstrates a clear excess in the energy region around 0.5 MeV in the case of neutron knockout, where a narrow $I^\pi = 1/2^-$ resonance was found ($E_r = 0.44(1)$ MeV, $\Gamma = 0.39(5)$ MeV [51]). The $I^\pi = 1/2^-$ state was not observed in the one-proton knockout from ^{14}B. The investigation of the ^{14}B structure, in studies of its Coulomb disintegration, favors $^{13}\mathrm{B}(3/2^-)\otimes 1s_{1/2}$ as the ground-state configuration with a spectroscopic factor close to unity [60]. This was confirmed in studies of the neutron-pickup reaction $^{13}\mathrm{B}(d, p)^{14}\mathrm{B}$, where the spectroscopic factors were found as 0.71 for the configura-

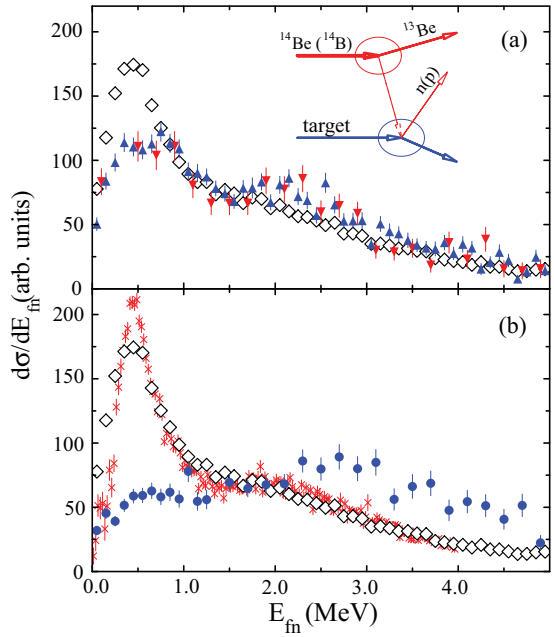

FIG. 7. (a) Relative-energy spectra ^{12}Be-n obtained in proton knockout from ^{14}B at 400 MeV/nucleon (▼, present data), and 35 MeV/nucleon (▲, Ref. [36]), and in neutron knockout from 360 MeV/nucleon ^{14}Be (◇, Ref. [51]). (b) Relative-energy spectra ^{12}Be-n in nucleon exchange with a ^{13}B beam (●, Ref. [37]), and in neutron knockout from ^{14}Be (◇, Ref. [51]; ×, Ref. [35]). All spectra were corrected for overall efficiencies of the experimental setup and normalized to the same integral in the relative-energy region 0–5 MeV.

tion ^{13}B$(3/2^-) \otimes 1s_{1/2}$, and 0.17 for ^{13}B$(3/2^-) \otimes 0d_{5/2}$. This indicates that, in the proton knockout from ^{14}B, the population of negative-parity states in ^{13}Be should be extremely rare [61]. The structure of the ^{14}Be(g.s.) wave function is expected to have an 85% ^{12}Be(p-shell) $\otimes (1s_{1/2})^2$ configuration, with a 15% ^{12}Be(p-shell) $\otimes (0d_{5/2})^2$ component [62]. Thus, a sudden neutron knockout from the ^{12}Be core results in a population of the negative-parity resonance $I^\pi = 1/2^-$ in ^{13}Be.

Figure 7(b) shows spectra obtained in a nucleon-exchange reaction [37]. This reaction could have populated states not populated in the nucleon-knockout reactions. A statement was made in Ref. [37] that the decay of the 2 MeV state does not have a branch with sequential decay through the 2^+ state in ^{12}Be, as was suggested in Ref. [51]. The conclusion made in Ref. [51] was, however, based on the measurements where the ^{12}Be-n spectrum was obtained in coincidence with the 2.1 MeV γ ray [35]. Two different fits to the experimental spectrum were done in Ref. [37], assuming two or three resonances. Both fits have the same statistical confidence level. The fit with three resonances was claimed to be in agreement with Ref. [36]. But the analysis made in Ref. [36] differs since the spectrum was decomposed into four different structures. References [36,37] show that relative-energy spectra can be understood in two or even several possible ways [38]. The spectrum obtained in the nucleon-exchange reaction is in Fig. 6(b) compared with those obtained in the neutron knockout at two different energies [31,46]. The difference in shape between the spectra from the two experiments is due to a superior energy resolution in the experiment with lower beam energy [31]. However, these two spectra differ qualitatively from the spectrum from the nucleon-exchange reaction. Excitation of the $1/2^+$ state is obviously strongly suppressed in the last case, as well as the $1/2^-$ state.

IV. SUMMARY

We presented an analysis of a one-proton-knockout experiment from 400 MeV/nucleon ^{14}B impinging on a CH_2 target. Triple coincidence data were collected, including ^{12}Be fragments, neutrons, and γ rays. The interpretation was performed by using already existing, published experimental data at lower energy. The partial level scheme of ^{13}Be is presented in Fig. 6. The following main conclusions can be drawn:

(i) Feeding of the ^{12}Be(2^+) state from neutron decay of the ^{13}Be$(5/2^+_1)$ state at 2.11 MeV was identified from triple coincidence data.
(ii) Evidence was found for an excited state in ^{13}Be at $E_r = 4$ MeV with two decay branches either to the ^{12}Be(g.s.) or to the ^{12}Be(2^+) state.
(iii) A simultaneous analysis of proton-knockout data at energies 35 and 400 MeV/nucleon give evidence for an energy independence of the proton-knockout mechanism.
(iv) A comparison between the spectra obtained in neutron knockout with those from a proton knockout confirms the excitation of the ^{13}Be$(1/2^-)$ state in the first case and negligible probability for population of negative-parity states in the second.
(v) The low-energy part of the ^{13}Be excitation spectrum is dominated by a very broad s-wave resonance $(1/2^+)$, extending from the ^{12}Be+n threshold to the top of the excitation spectrum, together with a rather narrow p-wave resonance $(1/2^-)$. To promote one of them as the ground state ^{13}Be is not within the scope of the present paper but certainly a challenge for theory.
(vi) The contradictions in the interpretations of the ^{13}Be structure obtained in experiments using the invariant-mass against the missing-mass methods is resolved by taking both methods into account in the analysis.
(vii) The results show that there is a danger in the interpretation of the invariant-mass data when the γ channel is not taken into account.

The ambiguity of the analysis can be eliminated only under the condition of measuring the decay branch with population of the isomeric ^{12}Be(0^+_2) state. The ^{13}Be$(5/2^+_2)$ state is expected to decay preferentially via the ^{12}Be(0^+_2) [54] and subsequently de-excite to ^{12}Be$(g.s)$ by emission of an e^+e^- pair [39,40]. The detection of annihilation γ rays from the state, with a lifetime of 331 ns, in coincidences with other reaction products, is indeed an experimental challenge.

Thus, considering that ^{12}Be is mostly ^{10}Be $\otimes (sd)^2$, in the reaction ^{12}Be$(d, p)^{13}$Be the states with the ^{10}Be $\otimes (sd)^3$ structures should be strongly excited. An interesting possibility to tackle this problem might come from the study of a two-neutron transfer reaction, ^{11}Be$(t, p)^{13}$Be [63].

ACKNOWLEDGMENTS

The authors are grateful to Y. Kondo for making available numerical data from the RIKEN experiment. G.R. acknowledges the predoctoral Grant No. BES-2010-042262 associated with the research project FPA2009-07387 funded by Ministerio de Ciencia e Innovación (Spain). This work has been partly supported by the Spanish Ministerio de Economía y Competitividad (MINECO) through Projects No. FPA2015-65035-P, No. FPA2012-32443, No. FPA2011-24553, No. FPA2011-29854-C04-01, No. FPA2013-41267-P, No. FPA2014-52823-C2-1-P, No. FPA2015-64969-P, and No. FPA2017-87568-P and by the European Union by means of the European Commission within its Seventh Framework Programme (FP7) via ENSAR (Contract No. 262010) and supported by NAVI, GSI-TU Darmstadt cooperation, HIC for FAIR, EMMI and BMBF, and from DFG through grant SFB1245 and Project No. 05P15RDFN1. C.A.B. acknowledges support by the U.S. DOE Grant No. DE-FG02-08ER41533 and the U.S. NSF Grant No. 1415656.

[1] V. Della Rocca and F. Iachello, Nucl. Phys. A **973**, 1 (2018).
[2] F. C. Barker, Phys. Rev. C **79**, 017302 (2009).
[3] V. D. Efros, H. Oberhummer, A. Pushkin, and I. Thompson, Eur. Phys. J. A **1**, 447 (1998).
[4] M. Odsuren, Y. Kikuchi, T. Myo, M. Aikawa, and K. Kato, Phys. Rev. C **92**, 014322 (2015).
[5] R. Alvarez-Rodriguez, A. S. Jensen, E. Garrido, and D. V. Fedorov, Phys. Rev. C **82**, 034001 (2010).
[6] E. Garrido, D. Fedorov, and A. S. Jensen, Phys. Lett. B **684**, 132 (2010).
[7] T. Myo, A. Umeya, H. Toki, and K. Ikeda, Prog. Theor. Exp. Phys. **2015**, 063D03 (2015).
[8] Yu. A. Lashko, G. F. Filippov, and V. S. Vasilevsky, Nucl. Phys. A **958**, 78 (2017).
[9] F. Kobayashi and Y. Kanada-En'yo, Phys. Rev. C **93**, 024310 (2016).
[10] D. H. Wilkinson and D. E. Alburger, Phys. Rev. **113**, 563 (1959).
[11] I. Talmi and I. Unna, Phys. Rev. Lett. **4**, 469 (1960).
[12] K. Riisager, Phys. Scr. T **152**, 014001 (2013).
[13] T. Aumann, A. Navin, D. P. Balamuth, D. Bazin, B. Blank, B. A. Brown, J. E. Bush, J. A. Caggiano, B. Davids, T. Glasmacher, V. Guimarães, P. G. Hansen, R. W. Ibbotson, D. Karnes, J. J. Kolata, V. Maddalena, B. Pritychenko, H. Scheit, B. M. Sherrill, and J. A. Tostevin, Phys. Rev. Lett. **84**, 35 (2000).
[14] J. S. Winfield *et al.*, Nucl. Phys. A **683**, 48 (2001).
[15] R. Crespo and E. Cravo, Few-Body Syst. **59**, 11 (2018).
[16] H. Sagawa, B. A. Browen, and H. Esbensen, Phys. Lett. B **309**, 1 (1993).
[17] A. Calci, P. Navratil, R. Roth, J. Dohet-Eraly, S. Quaglioni, and G. Hupin, Phys. Rev. Lett. **117**, 242501 (2016).
[18] F. C. Barker, J. Phys. G **2**, L45 (1976).
[19] A. Navin, D. W. Anthony, T. Aumann, T. Baumann, D. Bazin, Y. Blumenfeld, B. A. Brown, T. Glasmacher, P. G. Hansen, R. W. Ibbotson, P. A. Lofy, V. Maddalena, K. Miller, T. Nakamura, B. V. Pritychenko, B. M. Sherrill, E. Spears, M. Steiner, J. A. Tostevin, J. Yurkon, and A. Wagner, Phys. Rev. Lett. **85**, 266 (2000).
[20] G. F. Bertsch and H. Esbensen, Ann. Phys. (NY) **209**, 327 (1991).
[21] P. Descouvemont, Phys. Lett. B **331**, 271 (1994).
[22] I. J. Thompson and M. V. Zhukov, Phys. Rev. C **53**, 708 (1996).
[23] M. Labiche, F. M. Marques, O. Sorlin, and N. Vinh Mau, Phys. Rev. C **60**, 027303 (1999).
[24] J. C. Pacheco and N. Vinh Mau, Phys. Rev. C **65**, 044004 (2002).
[25] I. Hamamoto, Phys. Rev. C **77**, 054311 (2008).
[26] G. Blanchon, N. V. Mau, A. Bonaccorso, M. Dupuis, and N. Pillet, Phys. Rev. C **82**, 034313 (2010).
[27] H. T. Fortune, Phys. Rev. C **94**, 064308 (2016).
[28] H. T. Fortune, Phys. Rev. C **87**, 014305 (2013).
[29] H. T. Fortune, Eur. Phys. J. A **54**, 51 (2018).
[30] D. V. Aleksandrov *et al.*, Sov. J. Nucl. Phys. **37**, 474 (1983).
[31] A. N. Ostrowski *et al.*, Z. Phys. A **343**, 489 (1992).
[32] A. A. Korsheninnikov *et al.*, Phys. Lett. B **343**, 53 (1995).
[33] M. G. Gornov *et al.*, Bull. Russ. Acad. Sci. Phys. **62**, 1781 (1998).
[34] A. V. Belozyorov *et al.*, Nucl. Phys. A **636**, 419 (1998).
[35] Y. Kondo *et al.*, Phys. Lett. B **690**, 245 (2010).
[36] G. Randisi, A. Leprince, H. Al Falou, N. A. Orr, F. M. Marqués, N. L. Achouri, J.-C. Angélique, N. Ashwood, B. Bastin, T. Bloxham, B. A. Brown, W. N. Catford, N. Curtis, F. Delaunay, M. Freer, E. de Góes Brennand, P. Haigh, F. Hanappe, C. Harlin, B. Laurent, J.-L. Lecouey, A. Ninane, N. Patterson, D. Price, L. Stuttgé, and J. S. Thomas, Phys. Rev. C **89**, 034320 (2014).
[37] B. R. Marks, P. A. Deyoung, J. K. Smith, T. Baumann, J. Brown, N. Frank, J. Hinnefeld, M. Hoffman, M. D. Jones, Z. Kohley, A. N. Kuchera, B. Luther, A. Spyrou, S. Stephenson, C. Sullivan, M. Thoennessen, N. Viscariello, and S. J. Williams, Phys. Rev. C **92**, 054320 (2015).
[38] H. T. Fortune, Phys. Rev. C **93**, 054327 (2016).
[39] S. Shimoura *et al.*, Phys. Lett. B **560**, 31 (2003).
[40] S. Shimoura *et al.*, Phys. Lett. B **654**, 87 (2007).
[41] J. G. Johansen, V. Bildstein, M. J. G. Borge, M. Cubero, J. Diriken, J. Elseviers, L. M. Fraile, H. O. U. Fynbo, L. P. Gaffney, R. Gernhäuser, B. Jonson, G. T. Koldste, J. Konki, T. Kröll, R. Krücken, D. Mücher, T. Nilsson, K. Nowak, J. Pakarinen, V. Pesudo, R. Raabe, K. Riisager, M. Seidlitz, O. Tengblad, H. Törnqvist, D. Voulot, N. Warr, F. Wenander, K. Wimmer, and H. De Witte, Phys. Rev. C **88**, 044619 (2013).
[42] H. T. Fortune, Phys. Lett. B **755**, 351 (2016).
[43] S. G. Altstadt *et al.*, Nucl. Data Sheets **120**, 197 (2014).
[44] V. Metag *et al.*, in *Detectors in Heavy-Ion Reactions*, Lecture Notes in Physics Vol. 178 (Springer-Verlag, Berlin, 1983), pp. 163–178.
[45] R. Thies, Master's thesis, Chalmers University of Technology, 2011 (unpublished).
[46] Th. Blaich *et al.*, Nucl. Instrum. Methods Phys. Res. A **314**, 136 (1992).
[47] V. Panin *et al.*, Phys. Lett. B **753**, 204 (2016).
[48] A. M. Lane and R. G. Thomas, Rev. Mod. Phys. **30**, 257 (1958).
[49] F. James and M. Roos, Comput. Phys. Commun. **10**, 343 (1975).
[50] Yu. Aksyutina *et al.*, Phys. Lett. B **718**, 1309 (2013).
[51] Y. Aksyutina, T. Aumann, K. Boretzky, M. J. G. Borge, C. Caesar, A. Chatillon, L. V. Chulkov, D. Cortina-Gil, U. Datta Pramanik, H. Emling, H. O. U. Fynbo, H. Geissel, G. Ickert, H. T. Johansson, B. Jonson, R. Kulessa, C. Langer, T. LeBleis,

K. Mahata, G. Münzenberg, T. Nilsson, G. Nyman, R. Palit, S. Paschalis, W. Prokopowicz, R. Reifarth, D. Rossi, A. Richter, K. Riisager, G. Schrieder, H. Simon, K. Sümmerer, O. Tengblad, H. Weick, and M. V. Zhukov, Phys. Rev. C **87**, 064316 (2013).
[52] K. W. McVoy and P. Van Isaker, Nucl. Phys. A **576**, 157 (1994).
[53] H. T. Fortune, Phys. Rev. C **90**, 064305 (2014).
[54] H. T. Fortune and R. Sherr, Phys. Rev. C **82**, 064302 (2010).
[55] M. Thoennessen, S. Yokoyama, and P. G. Hansen, Phys. Rev. C **63**, 014308 (2000).
[56] G. Christian *et al.*, Nucl. Phys. A **801**, 101 (2008).
[57] J. L. Lecouey, Few-Body Syst. **34**, 21 (2004).
[58] H. Simon *et al.*, Nucl. Phys. A **791**, 267 (2007).
[59] M. A. Falou, A. Leprince, and N. Orr, Mod. Phys. Lett. A **25**, 1824 (2010).
[60] R. Chatterjee and P. Banerjee, Phys. Rev. C **63**, 017303 (2000).
[61] S. Bedoor, A. H. Wuosmaa, J. C. Lighthall, M. Alcorta, B. B. Back, P. F. Bertone, B. A. Brown, C. M. Deibel, C. R. Hoffman, S. T. Marley, R. C. Pardo, K. E. Rehm, A. M. Rogers, J. P. Schiffer, and D. V. Shetty, Phys. Rev. C **88**, 011304(R) (2013).
[62] H. T. Fortune, Phys. Rev. C **89**, 044312 (2014).
[63] M. J. G. Borge and K. Riisager, Eur. Phys. J. A **52**, 334 (2016).